Analysis of Flexibility and Hotspots in Bcl-xL and Mcl-1 Proteins for the Design of Selective Small-Molecule Inhibitors

Chao-Yie Yang and Shaomeng Wang*

Departments of Internal Medicine, Pharmacology, and Medicinal Chemistry, University of Michigan, 1500 East Medical Center Drive, Ann Arbor, Michigan 48109-0934, United States

S Supporting Information

ABSTRACT: Although Bcl-xL and Mcl-1, two antideath Bcl-2 members, have similar, flexible binding sites, they can achieve high binding selectivity to endogenous binding partners and synthetic small-molecule inhibitors. Here, we employed molecular dynamic (MD) simulations and hotspot analysis to investigate the conformational flexibility of these proteins and their binding hotspots at the binding sites. Backbone flexibility analyses indicate that the highest degree of flexibility in Mcl-1 is the $\alpha 4$ helical segment as opposed to the $\alpha 3$ helix in Bcl-xL among four helical segments in their binding sites. Furthermore, common and unique binding hotspots at both proteins were identified using small-molecule probes. These analyses can aid the design of potent and specific small-molecule inhibitors for these proteins.

KEYWORDS: Bcl-xL, Mcl-1, backbone flexibility, binding selectivity, cosolvent molecular dynamics simulation
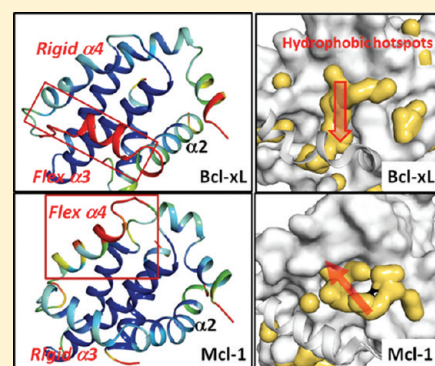
One major challenge in targeting protein−protein interactions (PPI) is that the interface between proteins is typically large and flexible,[1,2] and consequently, an in-depth understanding of how protein conformational flexibility governs both their binding affinity and specificity can aid the design of potent and specific small-molecule inhibitors of PPIs. The Bcl-2 proteins, a class of key regulators of programmed cell death, or apoptosis, are attractive cancer therapeutic targets.[3] The antiapoptotic members of this family including Bcl-2, Bcl-xL, Bcl-w, Bcl2A1, and Mcl-1 inhibit apoptosis via interaction with the BH3 (Bcl-2 homology 3) domain of pro-apoptotic Bcl-2 members. Available crystal structures[4−8] showed that the binding between the antideath and the pro-death Bcl-2 members is mediated by a large, hydrophobic groove in the antideath Bcl-2 proteins and a single acidic residue and four hydrophobic residues in the BH3 domain of the pro-death Bcl-2 proteins. The binding sites in the antideath Bcl-2 proteins involve four helical segments ($\alpha 2 - \alpha 5$) and exhibit significant conformational flexibility. Despite the similarity of the binding sites and their high conformational flexibility, these antideath Bcl-2 proteins also show high binding specificity to pro-death Bcl-2 proteins. For example, while Bcl-2 and Bcl-xL bind to Bad and Bim BH3 peptides with very high affinities, they have 1000 times weaker affinity to Noxa BH3 peptides.[9,10] Mcl-1 and Bcl2A1 bind to Bim and Noxa BH3 peptides with high affinities, whereas they have very weak affinities for Bad BH3 peptides (Table S1 in the Supporting Information). Similar to these BH3 peptides, nonpeptidic small-molecule inhibitors display high binding specificity to these antideath Bcl-2 proteins. For example, ABT-737 binds to Bcl-2, Bcl-xL, and Bcl-w with $K_i < 1$ nM but has >1000 times weaker affinity to

Mcl-1 and Bcl2A1.[11] Although amino acids in these BH3 peptides, which are key to their binding affinity and specificity to Bcl-xL, Bcl-2, Bcl-w, and Mcl-1, have recently been determined,[10] the reason why these antideath Bcl-2 proteins displays high binding specificity is not well understood.

In this study, we have investigated the conformational flexibility of apo-, holo-Bcl-xL/peptide and holo-Mcl-1/peptide and their binding sites using computational methods. Note that apo refers to the ligand-free protein structure, whereas holo-Bcl-xL/peptide refers to the peptide removed Bcl-xL conformation. Our study reveals that Bcl-xL and Mcl-1 have different backbone flexibilities with respect to their BH3 peptide binding sites despite their similarity. Both proteins also show distinct patterns of binding hotspots in their binding sites. Our study demonstrated that both aspects contribute to the binding specificity of the BH3 peptides to these structurally similar proteins.

To characterize and compare the backbone flexibility at the binding site of Bcl-xL with that of Mcl-1, we performed MD simulations of both proteins in water starting with Bcl-xL and Mcl-1 conformations with or without the peptide ligands. These included (a) apo-Bcl-xL, (b) holo-Bcl-xL/peptide, and (c) Bcl-xL/peptide (i.e., Bcl-xL bound with the peptide). The same notations for Mcl-1 are also used.

Although we performed 50 ns simulations started from each holo structure, they did not reach the conformational space

shown in the apo structure. Hence, the sampled conformations from different starting holo structures represent locally accessible microstates of the proteins when binding to different ligands. On the basis of these simulations, we assessed whether the binding site flexibility depends on different conformations of the protein structures and how ligand binding can affect binding site flexibility.

Order parameters of the backbone amide NH bond have been widely used in NMR spectroscopy[12] to give degrees of its angular motion for analyzing the backbone flexibility of the proteins. The value of order parameter decreases from one to zero corresponding to an increase in the protein backbone flexibility. Order parameters of the amide NH bond in each amino acid of Bcl-xL and Mcl-1 were calculated and are given in Figure 1. The potential energies of the proteins from the 50 ns
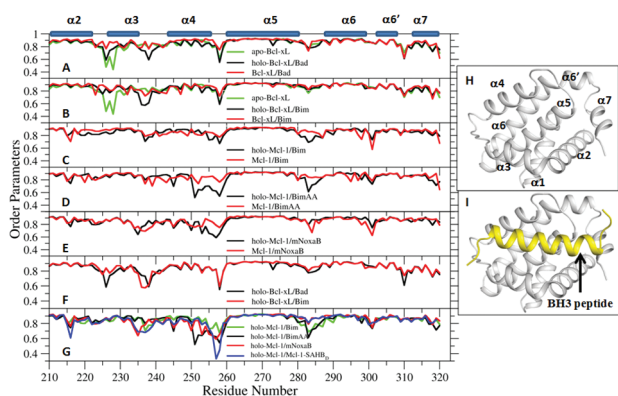
Figure 1. Calculated order parameters based on MD simulation in water using different conformations of holo-Bcl-xL/peptide (A, B, F) and holo-Mcl-1/peptide (C−E, G). Blue bars are helices in Bcl-xL and assigned in H. The residue number is based on Mcl-1. The BH3 Bim peptide at the binding site is shown in I. The results for apo-Bcl-xL, the protein/peptide complex simulations, and holo-proteins were from 1 to 50, 1 to 8, and 20 to 50 ns of MD simulations, respectively.

of MD simulations indicated that they are in equilibrated states (Figure S5 in the Supporting Information).

For Bcl-xL, we compared the order parameters of apo-Bcl-xL, holo-Bcl-xL/Bad, and Bcl-xL/Bad structures (Figure 1A) and those of apo-Bcl-xL, holo-Bcl-xL/Bim, and Bcl-xL/Bim structures (Figure 1B). Binding of both Bad and Bim to Bcl-xL significantly reduces the Bcl-xL backbone flexibility in the loop between the $\alpha2$ and $\alpha3$ helices, as compared to apo-Bcl-xL. For holo-Bcl-xL, higher degrees of flexibility in the loops between the $\alpha2$ and the $\alpha3$ helices and between the $\alpha3$ and the $\alpha4$ helices can be found when compared with the Bad/Bim-bound Bcl-xL. For Mcl-1, there is no experimentally determined apo structure. However, comparison of holo-Mcl-1/Bim versus Mcl-1/Bim, holo-Mcl-1/BimAA versus Mcl-1/BimAA, and holo-Mcl-1/mNoxaB versus Mcl-1/mNoxaB shows that binding of different ligands to Mcl-1 primarily reduces the protein backbone flexibility in the loop between the $\alpha4$ and the $\alpha5$ helices (Figure 1C−E). For holo-Mcl-1/mNoxaB, the loop between the $\alpha3$ and the $\alpha4$ helices showed higher flexibility than those of the holo-Mcl-1/Bim and holo-Mcl-1/BimAA. This signature was observed for another selective Mcl-1-SAHB$_D$ peptide to Mcl-1 (Figure 1G). Mcl-1-SAHB$_D$ is a modified peptide derived from the BH3 domain of Mcl-1 that binds selectively to Mcl-1 with a K_D value of 10 nM.[13] The higher flexibility in the loop between the $\alpha3$ and the

$\alpha4$ helices of the holo-Mcl-1/mNoxaB and holo-Mcl-1/Mcl-1-SAHB$_D$ is not specific to Mcl-1. It was also observed in holo-Bcl-xL (cf. Figure 1F vs G) and is attributed to the flexible nature of the loop region in both proteins.

The comparison showed that Bcl-xL has higher backbone flexibility in two loops flanking the $\alpha3$ helix than that in other helices, while Mcl-1 is more flexible in the loop between the $\alpha4$ and the $\alpha5$ helices (Figure 1A−E). The higher degree of backbone flexibility around the $\alpha3$ helix in Bcl-xL revealed in our simulations can contribute to the changes of the length and conformation of the $\alpha3$ helix in Bcl-xL when binding to the peptide ligands as observed in the crystal structures.[14] In contrast, only one loop between $\alpha3$ and $\alpha4$ in Mcl-1 showed a higher degree of backbone flexibility, which imposes a limit to the conformational changes of the $\alpha3$ helix in Mcl-1. Analysis of the structures between Mcl-1 and different peptides has indicated no major conformational differences found with respect to the Mcl-1 binding site.[15]

Interestingly, our simulation showed that the $\alpha4$ segment in holo-Mcl-1/Bim partially unfolds, converting a complete helix into two shorter helices (Figure 2A,B) and so shields the
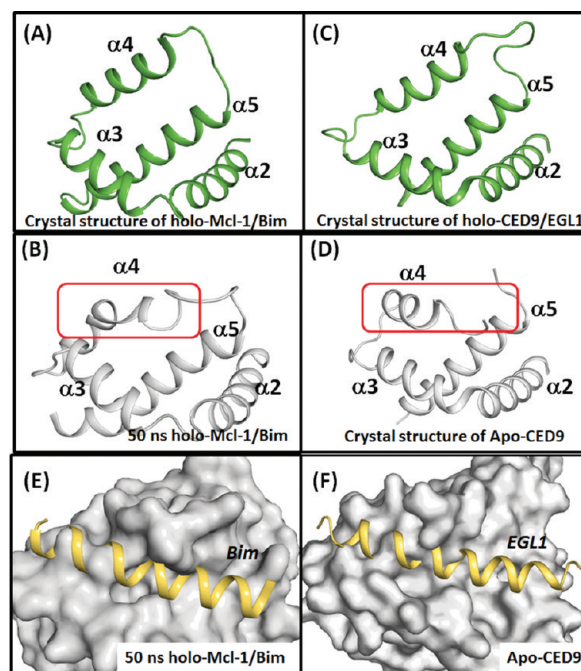
Figure 2. (A) Crystal structure of holo-Mcl-1/Bim and (B) the conformation of the holo-Mcl-1/Bim after 50 ns of MD simulation in water. Crystal structures of (C) holo-CED9/EGL1 (PDB: 1TY4) and (D) apo-CED9 (1OHU). A loop segment between $\alpha4$ and $\alpha5$ in CED9 is disordered and not resolved in the crystal structure. Only $\alpha2-\alpha5$ helices were shown for clarity. The 50 ns holo-Mcl-1/Bim and apo-CED9 were aligned with holo-Mcl-1/Bim and holo-CED9/EGL1, respectively, to give the structures of the Bim and EGL1 peptides in E and F. The PyMOL program (www.pymol.org) was used to prepare the graphics.

hydrophobic binding groove from water molecules (Figure 2E). Although no apo-Mcl-1 structure is available to confirm this observation, we noted that the orthologue of the Bcl-2 family protein in *C. elegans*, CED9, indeed adopts a similar fold topology in its apo-form. Part of the $\alpha4$ helix in apo-CED9 is disordered and shields the hydrophobic pocket (Figure 2D). When bound to EGL-1 (an orthologue of the BH3-only
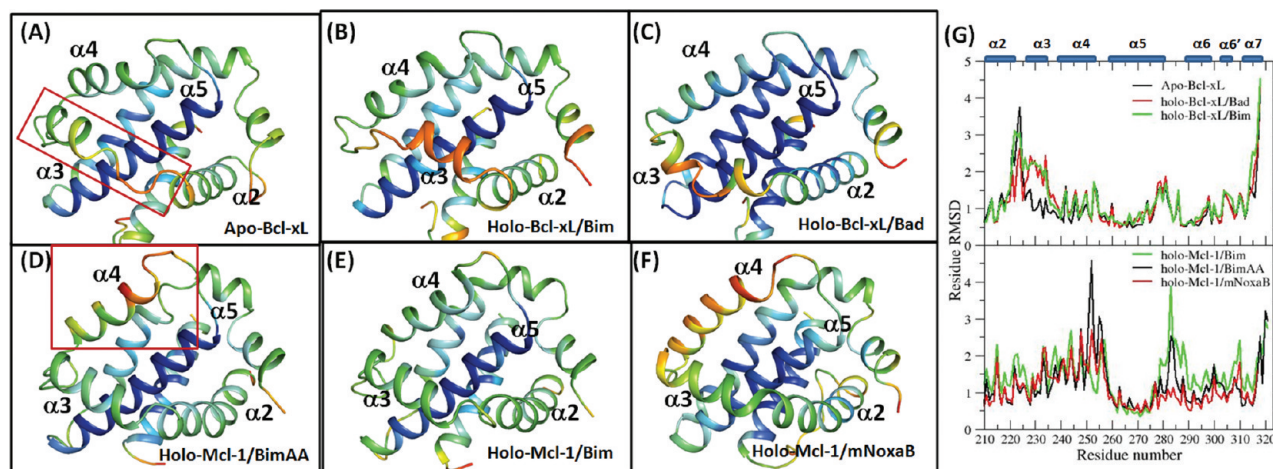
Figure 3. Calculated pRMSD of (A) apo-Bcl-xL, (B) holo-Bcl-xL/Bim, (C) holo-Bcl-xL/Bad, (D) holo-Mcl-1/BimAA, (E) holo-Mcl-1/Bim, and (F) holo-Mcl-1/mNoxaB from the 50 ns MD simulations in water (G). The color changes from blue to red as the values of pRMSD increase. Regions of distinctive backbone flexibility between holo-Bcl-xL/peptide and holo-Mcl-1/peptide are enclosed by red boxes. The crystal structures of the proteins were used as the reference structures.

proteins), folding of a longer $\alpha4$ helix of holo-CED9/EGL-1 is induced, exposing a hydrophobic groove for interaction with the BH3 domain of EGL-1 (Figure 2C), similar to the conformation of Mcl-1 interacting with the BH3 peptides. An example of holo-Mcl-1/Bim is shown in Figure 2A. Ramachandran plots of the conformations of the apo-Bcl-xL, holo-Bcl-xL, and holo-Mcl-1 at 50 ns are provided in Figure S1 in the Supporting Information.

We further analyzed the residue flexibility of Bcl-xL and Mcl-1 proteins by calculating the positional root-mean squared deviation (pRMSD) of heavy atoms from that in the static crystal structure using the ensemble of protein conformations obtained from the simulations (see Figure 3G). Large values of pRMSD correspond to greater positional movement of the atoms and thus a more flexible protein chain. The results are shown in Figure 3 depicted by a change of backbone color from blue to red, denoting an increased pRMSD. For apo-Bcl-xL, large pRMSDs are observed in the loop between $\alpha2$ and $\alpha3$ helices (Figure 3A). Both holo-Bcl-xL/Bim (Figure 3B) and holo-Bcl-xL/Bad (Figure 3C) conformations showed greater pRMSDs in the $\alpha3$ helix whose movement results in the concealing of the hydrophobic binding site. Large pRMSDs of the $\alpha3$ helix in holo-Bcl-xL/Bim are attributed to movement of the entire $\alpha3$ helix anchored by the loop between the $\alpha3$ and the $\alpha4$ helices (Figure 3B) because no structure changes were observed in the $\alpha3$ helix during simulations (Figure S2 in the Supporting Information). For holo-Mcl-1/peptide conformations, large pRMSDs are found mainly at the $\alpha4$ helix and the loop between $\alpha4$ and $\alpha5$ helices (Figure 3D−F). Although the dynamical motion of the loop between the $\alpha4$ and the $\alpha5$ helices in holo-Mcl-1/Bim is less pronounced, monitoring the helical conformation at the $\alpha4$ helix (Figure S3 in the Supporting Information) and the protein conformations confirmed their similar flexibility with holo/BimAA. In contrast to holo-Bcl-xL/peptide, the $\alpha3$ helix remains rigid in all three of the holo-Mcl-1/peptide conformations. Although the crystal structures of holo-Bcl-xL clearly indicated the high flexibility of its $\alpha3$ helix upon ligand binding, the holo-Mcl-1 crystal structures did not reveal the high flexibility of its $\alpha4$ helix. Our MD simulations thus revealed the high flexibility of $\alpha4$ helix in Mcl-1 and suggested that holo-Bcl-xL/peptide and holo-Mcl-1/

peptide use $\alpha3$ and $\alpha4$ helices, respectively, to conceal the hydrophobic groove that interacts with the BH3 peptides.

We next probed the binding hotspots in Bcl-xL and Mcl-1 by taking account of their high conformational flexibility. To prevent the hydrophobic collapse of the large, flexible, and hydrophobic binding pockets in Bcl-xL and Mcl-1 when simulating their holo-structures in water, we employed a recently developed cosolvent simulation method.[14,16,17] Cosolvent simulations provide a convenient way to probe the binding hotspots via analysis of the interactions between the cosolvent molecules and the protein,[14,16,17] while accounting for the conformational flexibility contributed collectively by the backbone and side chain atoms of the proteins at the binding site.

The hydrophobic and acidic hotspots were identified using isopropanol (20% v/v), phenol (10% v/v), and 2 M trimethylamine N-oxide (TMAO) to represent saturated (C.3) and aromatic (C.ar) carbon atoms and acidic oxygen atom probes, respectively, in the cosolvent simulations. Rationales are provided in the Supporting Information. As described previously,[14,17] the chemical graphs derived from the cosolvent mapping analyses are influenced by the types of probe atoms used, and the locations of the probe atoms represent the hotspots attributed to a favored interaction between the proteins and the probes.

In Figure 4, the h1, h2, h3, h4, and p1 sites refer to the docked positions of four hydrophobic residues (I90, L94, I97, and F101) and the single charged residue (D99) on the Bim BH3 peptide that interact with proteins. For holo-Bcl-xL/Bim and holo-Mcl-1/Bim, the hydrophobic hotspots detected by both C.3 (i.e., the two methyl carbon atoms in isopropanol) and C.ar (i.e., the ring carbon atoms of phenol) atoms formed larger clusters at the h2 and h4 sites in both holo-Bcl-xL/Bim and holo-Mcl-1/Bim (Figure 4B,E). While more hydrophobic hotspots were detected at the h3 site in holo-Mcl-1/Bim than in holo-Bcl-xL/Bim, the hotspots close to the h1 site were found in holo-Bcl-xL/Bim but not in holo-Mcl-1/Bim. Thus, for binding to the same nonselective and potent Bim BH3 peptide, the h2 and h4 sites in Bcl-xL and Mcl-1 are the common dominant contributors to the binding. The saturated carbon group at the h4 site is more favored in Mcl-1 (see the
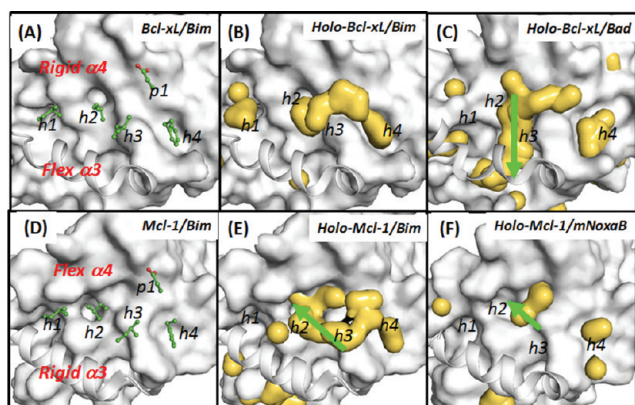
Figure 4. Hydrophobic hotspot distributions shown as yellow enveloped surfaces in holo-Bcl-xL/peptide and holo-Mcl-1/peptide. Analyses are based on 16 ns cosolvent simulations of the (B) holo-Bcl-xL/Bim and (C) holo-Bcl-xL/Bad and those of the (E) holo-Mcl-1/Bim and (F) holo-Mcl-1/mNoxaB from the crystal structures. Probe molecules include 20% isopropanol and 10% phenol v/v. The reference structures used in the surface representation are the crystal structures of Bcl-xL/peptide and Mcl-1/peptide. Key Bim residues are shown in green stick models in A and B. Important hydrophobic binding sites are labeled as h1−h4 and a single polar site as p1. Hotspots were defined as the ΔG of pseudo atoms < −1.0 kcal/mol.

Supporting Information). Additional common hydrophobic binding hotspots were found in the region connecting the h2 and the h4 sites of holo-Bcl-xL/Bim and holo-Mcl-1/Bim.

Next, we compared Bcl-xL and Mcl-1 bound with two selective BH3 peptides, namely, Bad and mNoxaB. For holo-Bcl-xL/Bad, the h1 site is much less important than the h2−h4 sites because of absence of hotspots detected in holo-Bcl-xL/Bad. However, a distinctive hotspot region penetrating downward at the h2 site was found in holo-Bcl-xL/Bad (indicated by the green arrow in Figure 4C). This hotspot region has also been identified in the apo-Bcl-xL and holo-Bcl-xL/Bec1 conformations previously.[14] For holo-Mcl-1/mNoxaB, hotspot regions were detected mostly at the h2 site and secondarily at the h4 site (Figure 4F). Hotspots detected at the h2 site in holo-Mcl-1/Bim and holo-Mcl-1/mNoxaB were both found to penetrate into the h2 site (arrows in Figure 4E,F), which was buried in the surface representation of the crystal structures in Figure 4.

Distinctive differences in the hydrophobic hotspot distributions at the h2 and h3 sites of holo-Bcl-xL/peptide and holo-Mcl-1/peptide indicated by the arrows in Figure 4 can be clearly seen. They are reminiscent of the different binding site flexibility of the holo-protein simulations described above. The flexible α3 helix in Bcl-xL adopts a distorted helix conformation, which allows the selective Bad peptide to access the hydrophobic hotspots downward from the h2 site. The same region is not accessible in holo-Mcl-1/peptide (Figure 4E,F) because of its rigid α3 helix. The backbone flexibility differences of the α3 helix between Bcl-xL and Mcl-1 are responsible in part for the failure of the bulky Tyr90 in the Bad peptide being tolerated in Mcl-1, while it is accommodated in Bcl-xL. The cosolvent mapping on both the holo-Mcl-1/Bim and the holo-Mcl-1/mNoxaB conformations identifies hotspot regions penetrating deeper into the h2 site (Figure 4E,F), hotspots absent from holo-Bcl-xL/peptide. This additional hotspot region in Mcl-1 is attributed to a pocket formed resulting from a kinked α4 helix conformation in the holo-Mcl-

1/peptide conformations. This pocket is generally absent in the holo-Bcl-xL/peptide conformations (Figure 4B,C).

Using TMAO as the probe molecule, we detected acidic hotspots close to the p1 site in both the holo-Bcl-xL/Bim and the holo-Bcl-xL/Bad conformations from the 1−16 ns of simulations (Figure 5A,B). Similar hotspots to the p1 site were
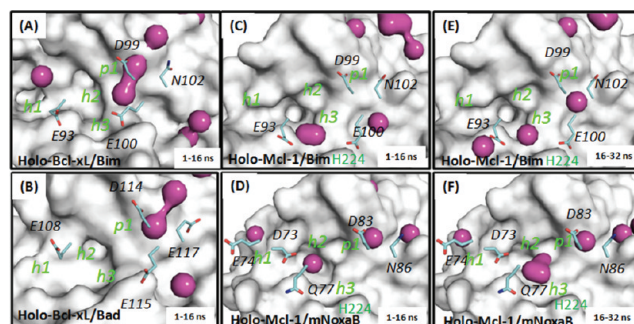
Figure 5. Acidic hotspots (purple) distributions in (A) holo-Bcl-xL/Bim, (B) holo-Bcl-xL/Bad, (C) holo-Mcl-1/Bim, and (D) holo-Mcl-1/mNoxaB determined by the oxygen atom of TMAO from the cosolvent simulations in 2 M TMAO. Amino acids with oxygen atoms at the side chain of the BH3 peptides were shown in the stick model and labeled.

detected in holo-Mcl-1/mNoxaB during 1−16 and 16−32 ns of simulations (Figure 5D,F). The acidic hotspot at the p1 site in holo-Mcl-1/Bim was detected in 16−32 ns of simulations (Figure 5E) but not in the first 16 ns simulation (Figure 5C). Because D99 of the Bim peptide at the p1 site interacts with R139 in Bcl-xL or R263 in Mcl-1, Figure 5 suggests a greater degree of side chain motion of Arg in holo-Mcl-1/Bim than in holo-Bcl-xL/Bim. The identified acidic hotspots also indicate that the h2 site in holo-Mcl-1/peptide is more receptive to polar groups than the corresponding site in holo-Bcl-xL/peptide. This is consistent with the fact that mutation of L94 (docked to the h2 site) in Bim BH3 peptide to polar amino acids, such as Gln, Asn, yielded IC_{50} values lower by a factor of 10 with Mcl-1 but by factors of more than 1000 with Bcl-xL.[18] An acidic hotspot in the h3 site of holo-Mcl-1/Bim is found close to H224 in Mcl-1. H224 in Mcl-1 is not conserved in either Bcl-2 or Bcl-xL in which the corresponding residue is Y101. Hence, our analyses of acidic hotspots in Bcl-xL and Mcl-1 indicate that the acidic amino acids in the BH3 peptides do not contribute directly to the selectivity of Bad and Noxa with both proteins.

In summary, our MD simulations in water identify that the α3 helix in Bcl-xL is highly flexible, whereas only the α4 helix in Mcl-1 is very flexible among the four helices forming the binding site. The flexible segment in Mcl-1 has not been identified from previously reported crystal structures. Cosolvent mapping analysis indicates common hydrophobic binding hotspots at h2 and h4 sites in both Bcl-xL and Mcl-1. However, binding hotspot distributions between Bcl-xL and Mcl-1 at the h2 sites differ. Binding hotspots penetrated downward at the h2 site for Bcl-xL whereas inward at the h2 site for Mcl-1. At the h4 site, a larger hydrophobic moiety consisting of either saturated or aromatic carbon atoms is favored by Bcl-xL, but a fragment of saturated carbon atoms appears to be more suitable for Mcl-1. Acidic hotspots at the p1 site are important for Bcl-xL and Mcl-1, but the mobility of the interacting Arg from Mcl-1 is higher than the same residue in Bcl-xL. The h2 and h3 sites

in Mcl-1 are also more receptive to polar atoms than those in Bcl-xL. They are attributed in part to the distinct conformational flexibility contributed by both backbone and side chain atoms in their binding sites. Our study suggests that exploration of the backbone flexibility and both common and different hotspots in these proteins may lead to the design of potent and selective, nonpeptide small-molecule inhibitors for these important apoptosis regulators.

■ ASSOCIATED CONTENT

Ⓢ Supporting Information

Material detailing the computational methods. This material is available free of charge via the Internet at http://pubs.acs.org.

■ AUTHOR INFORMATION

Corresponding Author

*Tel:+1-734-615-0362. Fax: +1-734-647-9647. E-mail: shaomeng@umich.edu.

Notes

The authors declare no competing financial interest.

■ ACKNOWLEDGMENTS

■ REFERENCES

(1) Berg, T. Small-molecule inhibitors of protein-protein interactions. *Curr. Opin. Drug Discovery Dev.* **2008**, *11*, 666−674.

(2) Wells, J. A.; McClendon, C. L. Reaching for high-hanging fruit in drug discovery at protein-protein interfaces. *Nature* **2007**, *450*, 1001−1009.

(3) Youle, R. J.; Strasser, A. The BCL-2 protein family: Opposing activities that mediate cell death. *Nat. Rev. Mol. Cell Biol.* **2008**, *9*, 47−59.

(4) Sattler, M.; Liang, H.; Nettesheim, D.; Meadows, R. P.; Harlan, J. E.; Eberstadt, M.; Yoon, H. S.; Shuker, S. B.; Chang, B. S.; Minn, A. J.; Thompson, C. B.; Fesik, S. W. Structure of Bcl-xL-Bak peptide complex: Recognition between regulators of apoptosis. *Science* **1997**, *275*, 983−986.

(5) Petros, A. M.; Nettesheim, D. G.; Wang, Y.; Olejniczak, E. T.; Meadows, R. P.; Mack, J.; Swift, K.; Matayoshi, E. D.; Zhang, H.; Thompson, C. B.; Fesik, S. W. Rationale for Bcl-xL/Bad peptide complex formation from structure, mutagenesis, and biophysical studies. *Protein Sci.* **2000**, *9*, 2528−2534.

(6) Liu, X.; Dai, S.; Zhu, Y.; Marrack, P.; Kappler, J. W. The structure of a Bcl-xL/Bim fragment complex: implications for Bim function. *Immunity* **2003**, *19*, 341−352.

(7) Lee, E. F.; Sadowsky, J. D.; Smith, B. J.; Czabotar, P. E.; Peterson-Kaufman, K. J.; Colman, P. M.; Gellman, S. H.; Fairlie, W. D. High-resolution structural characterization of a helical alpha/beta-peptide foldamer bound to the anti-apoptotic protein Bcl-xL. *Angew. Chem., Int. Ed. Engl.* **2009**, *48*, 4318−4322.

(8) Oberstein, A.; Jeffrey, P. D.; Shi, Y. Crystal structure of the Bcl-XL-Beclin 1 peptide complex: Beclin 1 is a novel BH3-only protein. *J. Biol. Chem.* **2007**, *282*, 13123−13132.

(9) Chen, L.; Willis, S. N.; Wei, A.; Smith, B. J.; Fletcher, J. I.; Hinds, M. G.; Colman, P. M.; Day, C. L.; Adams, J. M.; Huang, D. C. Differential targeting of prosurvival Bcl-2 proteins by their BH3-only ligands allows complementary apoptotic function. *Mol. Cell* **2005**, *17*, 393−403.

(10) Dutta, S.; Gulla, S.; Chen, T. S.; Fire, E.; Grant, R. A.; Keating, A. E. Determinants of BH3 binding specificity for Mcl-1 versus Bcl-xL. *J. Mol. Biol.* **2010**, *398*, 747−762.

(11) Oltersdorf, T.; Elmore, S. W.; Shoemaker, A. R.; Armstrong, R. C.; Augeri, D. J.; Belli, B. A.; Bruncko, M.; Deckwerth, T. L.; Dinges, J.; Hajduk, P. J.; Joseph, M. K.; Kitada, S.; Korsmeyer, S. J.; Kunzer, A. R.; Letai, A.; Li, C.; Mitten, M. J.; Nettesheim, D. G.; Ng, S.; Nimmer, P. M.; O'Connor, J. M.; Oleksijew, A.; Petros, A. M.; Reed, J. C.; Shen, W.; Tahir, S. K.; Thompson, C. B.; Tomaselli, K. J.; Wang, B.; Wendt, M. D.; Zhang, H.; Fesik, S. W.; Rosenberg, S. H. An inhibitor of Bcl-2 family proteins induces regression of solid tumours. *Nature* **2005**, *435*, 677−681.

(12) Lee, A. L.; Wand, A. J. Nuclear Magnetic Resonance (NMR) Spectroscopy for Monitoring Molecular Dynamics in Solution. *eLS*; John Wiley & Sons, Ltd.: Hoboken, NJ, 2001.

(13) Stewart, M. L.; Fire, E.; Keating, A. E.; Walensky, L. D. The MCL-1 BH3 helix is an exclusive MCL-1 inhibitor and apoptosis sensitizer. *Nat. Chem. Biol.* **2010**, *6*, 595−601.

(14) Yang, C.-Y.; Wang, S. Hydrophobic Binding Hot Spots of Bcl-xL Protein−Protein Interfaces by Cosolvent Molecular Dynamics Simulation. *ACS Med. Chem. Lett.* **2011**, *2*, 280−284.

(15) Fire, E.; Gulla, S. V.; Grant, R. A.; Keating, A. E. Mcl-1-Bim complexes accommodate surprising point mutations via minor structural changes. *Protein Sci.* **2010**, *19*, 507−519.

(16) Seco, J.; Luque, F. J.; Barril, X. Binding site detection and druggability index from first principles. *J. Med. Chem.* **2009**, *52*, 2363−2371.

(17) Yang, C.-Y.; Wang, S. Computational Analysis of Protein Hotspots. *ACS Med. Chem. Lett.* **2010**, *1*, 125−129.

(18) Lee, E. F.; Czabotar, P. E.; Smith, B. J.; Deshayes, K.; Zobel, K.; Colman, P. M.; Fairlie, W. D. Crystal structure of ABT-737 complexed with Bcl-xL: implications for selectivity of antagonists of the Bcl-2 family. *Cell Death Differ.* **2007**, *14*, 1711−1713.